Neuroradiology (2002) 44: 656–666
DOI 10.1007/s00234-002-0816-9

D. Yang
Y. Korogi
T. Sugahara
M. Kitajima
Y. Shigematsu
L. Liang
Y. Ushio
M. Takahashi

Cerebral gliomas: prospective comparison of multivoxel 2D chemical-shift imaging proton MR spectroscopy, echoplanar perfusion and diffusion-weighted MRI

Received: 30 January 2002
Accepted: 10 April 2002
Published online: 29 June 2002

D. Yang · Y. Korogi (✉) · T. Sugahara
M. Kitajima · Y. Shigematsu
L. Liang · M. Takahashi
Department of Radiology,
Kumamoto University School of Medicine,
1-1-1 Honjo, Kumamoto 860-8556, Japan
E-mail:
yuku@kaiju.medic.kumamoto-u.ac.jp
Tel.: +81-96-3735261
Fax: +81-96-3624330

Y. Ushio
Department of Neurosurgery,
Kumamoto University School of Medicine,
1-1-1 Honjo, Kumamoto 860-8556, Japan

D. Yang
Pittsburgh NMR Center for Biomedical
Research, Carnegie Mellon University,
Pittsburgh, PA 15213-2683, USA

Abstract Developments in MRI have made it possible to use diffusion-weighted MRI, perfusion MRI and proton MR spectroscopy (MRS) to study lesions in the brain. We evaluated whether these techniques provide useful, complementary information for grading gliomas, in comparison with conventional MRI. We studied 17 patients with histologically verified gliomas, adding multivoxel proton MRS, echoplanar diffusion and perfusion MRI the a routine MRI examination. The maximum relative cerebral blood volume (CBV), minimum apparent diffusion coefficient (ADC) and metabolic peak area ratios in proton MRS were calculated in solid parts of tumours on the same slice from each imaging data set. The mean minimum ADC of the 13 high-grade gliomas ($0.92 \pm 0.27 \times 10^{-3}$ mm^2/s) was lower than that of the four low-grade gliomas ($1.28 \pm 0.15 \times 10^{-3}$ mm^2/s) ($P < 0.05$). Means of maximum choline (Cho)/N-acetylaspartate (NAA), Cho/creatine (Cr), Cho/Cr in normal brain (Cr-n) and minimum NAA/Cr ratios were 5.90 ± 2.62, 4.73 ± 2.22, 2.66 ± 0.68 and 0.40 ± 0.06, respectively, in the high-grade gliomas, and 1.65 ± 1.37, 1.84 ± 1.20, 1.61 ± 1.29 and 1.65 ± 1.61, respectively, in the low-grade gliomas. Significant differences were found on spectroscopy between the high- and low-grade gliomas ($P < 0.05$). Mean maximum relative CBV in the high-grade gliomas (6.10 ± 3.98) was higher than in the low-grade gliomas (1.74 ± 0.57) ($P < 0.05$). Echoplanar diffusion, perfusion MRI and multivoxel proton MRS can offer diagnostic information, not available with conventional MRI, in the assessment of glioma grade.

Keywords Brain neoplasms · Magnetic resonance imaging · Diffusion · Perfusion · Magnetic resonance spectroscopy

Introduction

Gliomas, the most frequent primary brain tumours, are histologically heterogeneous, representing a biologic continuum with varying degrees of cellular and nuclear pleomorphism, mitotic activity, vascular proliferation and necrosis. Each type of glioma can be of low- or high-grade malignancy. Despite aggressive treatment, the prognosis of malignant gliomas is generally poor, because of their infiltrative nature and high relapse rate [1]. Because the therapeutic approaches for these tumours differ considerably according to tumour grade, the development of in vivo techniques which allow accurately determination of the grade would be important for determining appropriate treatment. A sampling error at limited biopsy may mean that the specimen does not reflect the degree of malignancy elsewhere in the tumour and may result in significant undergrading [2]. Preoperative grading of glioma helps in better treatment planning and management [3, 4].

Although conventional MRI with gadolinium-containing contrast media has been useful for characterising brain tumours [5], areas of contrast enhancement are not always the most malignant portion of the tumour, because some low-grade tumours show contrast enhancement and a few glioblastomas do not [6, 7]. High- and low-grade tumours cannot therefore be reliably differentiated on the basis of contrast enhancement. Abnormal signal around tumours on T2-weighted images is nonspecific, since it can represent neoplastic infiltration, vasogenic oedema or frequently both [7].

The data provided by proton MR spectroscopy (MRS), perfusion and diffusion-weighted imaging (DWI) are independent of each other, but complementary to MRI. Regional cerebral blood volume (CBV) maps calculated from MR images are particularly sensitive to the microvasculature and can enable detection of neovascularisation at the capillary level, and its relative quantification terms [8, 9]. Diffusion-weighted MRI reflects the physicochemical properties of the tissue (e.g., viscosity and temperature) as well as its structural components (macromolecules, membranes and intracellular organelles) [10]. MRS provides biochemical information on pathophysiology changes at the cellular level [11].

Although single-voxel MRS has been reported to be useful for investigation of gliomas [12], it is difficult to assess the spatial distribution of spectral changes. Recent developments in MRS have made it possible to obtain chemical-shift imaging (CSI) with high spatial resolution and multiple spectra simultaneously from contiguous voxels [13, 14]. Considering tumour inhomogeneity and partial volume effects, CSI may be more useful than single-voxel techniques for showing abnormal choline (Cho) levels [15].

To our knowledge, a combination of perfusion, DWI and proton MRS has not been used to assess brain tumours. One study verified that the combination of proton MRS and haemodynamic MRI could be used to characterise childhood brain tumours [16], and another demonstrated a significant inverse correlation between apparent diffusion coefficients (ADC) and Cho signal intensities [17], although both studies included patients who had undergone radiotherapy before the MRI.

The purposes of this study were to evaluate whether DWI, perfusion MRI and multivoxel MRS can provide useful, complementary information for grading of cerebral gliomas in addition to that given by conventional MRI, and to look for correlations between the various techniques.

Materials and methods

We studied 17 patients, 11 male and 6 female, with supratentorial gliomas of varying grade and type, aged 14–67 years. None had undergone chemo- or radiotherapy or surgery. We carried out surgery to remove the tumour in 14 cases within 10 days of the MRI. In cases 7, 8 and 9 the diagnosis was histologically verified by stereotactic biopsy. The malignancy of the gliomas was graded from 1 to 4, according to the World Health Organisation system. The diagnoses were glioblastoma (eight cases), anaplastic astrocytoma (two), anaplastic oligoastrocytoma (three), low-grade astrocytoma (two), and oligoastrocytoma and subependymal giant cell astrocytoma associated with tuberous sclerosis in one case each.

Conventional MRI, DWI, multivoxel proton MRS and perfusion imaging were acquired during the same procedure to allow exact comparison of the results. We used a 1.5 tesla superconducting system with 25 mT/m maximum gradient capability and a standard head coil.

After T1-weighted localising images, we acquired axial T1- and T2-weighted images. T1-weighted images were obtained with field of view (FOV) 20×20 cm, TR 670, TE 14 ms, one excitation, 256×256 matrix, 5-mm-thick sections with 1-mm intersection gap and acquisition time of 2 min 32 s and T2-weighted fast spin-echo images with FOV 20×20 cm, TR 3700, TE 96 ms, echo-train length 7, one excitation, 256×256 matrix, 5-mm sections with 1-mm intersection gap and acquisition time 2 min 7 s. Then, we obtained axial DWI, followed by multivoxel 2D CSI proton MRS. A 21-gauge needle was inserted in the right antecubital vein, and a bolus of gadopentetate dimeglumine (Gd-DTPA) was injected manually, after which we obtained a regional map of relative cerebral blood volume (CBV). Finally, we obtained contrast-enhanced axial T1-weighted images.

The conventional images were analysed independently by two neuroradiologists (D.Y., Y.K.), with consensus if there was disagreement. The images were analysed for the presence of necrosis, contrast enhancement, distant tumour foci, heterogeneity, cyst formation and definition of the borders of the tumour.

We used a multisection spin-echo echoplanar (EPI) sequence combining the motion-probing gradients (MPG) before and after the 180° pulse with EPI readout was used for intravoxel incoherent motion (IVIM) DWI. The diffusion gradient was three in directions (x, y and z-axes). The sequence was modified by adding large MPG pulses on both sides of the 180° pulse sequence along the three orthogonal directions for each section. The signal intensity obtained with diffusion weighting S_b is determined according to the equation,

$$S_b = So\ \exp\left[-\gamma^2 G^{2d2}(\Delta - \delta/3)ADC\right] = So\ \exp(-b\ ADC) \qquad (1)$$

where γ is the gyromagnetic ratio; δ the duration of each diffusion gradient; Δ the time between the onset of the diffusion gradient pulses; G the gradient strength; So the signal intensity without diffusion weighting; and b the diffusion-weighted factor. Sequential sampling of k-space was used, with TR 4700, TE 118 ms, bandwidth 830 Hz per pixel, and 128 lines of data acquired in 0.3 s. The other imaging conditions were FOV 22×22 cm, 96×128 matrix, 5-mm sections and one excitation. DWI was carried out with fat suppression by placing a frequency-selective radiofrequency (RF) pulse before the pulse sequence. For the images acquired in this study, δ was 26 ms, Δ 59.7 ms and G 20.1 mT/M, resulting in values for the gradient factor b of 1000 s/mm^2.

ADC were calculated for each of the three axes (x, y, z) of the column of interest according to the formula $ADC = -(1/b)\ln(S_b / S_0)$, where S_0 is the signal intensity without diffusion weighting and S_b the signal intensity with diffusion weighting. From these data, an average ADC [18, 19] in the three orthogonal directions was calculated on a pixel-by-pixel basis, using the equation

$$ADC_{av} = 1/3 \sum_{i=x,y,z} ADC_b \qquad (2)$$

where x, y, z are the directions of diffusion weighting and ADC_{av} is the average ADC. DWI produced by MPG pulse and ADC maps

reflecting ADC at each pixel were obtained. Analysis of the DWI was performed by placing regions of interest (ROI) over more than five areas within the tumours. The ROI, with >10 pixels, were carefully placed so that they did not include large areas of fluid which would appear to represent cysts or necrosis. Then the minimum mean ADC were selected.

In all patients, regional CBV maps were obtained with gradient-echo (GE) EPI at a readout bandwidth of 926 Hz per pixel, and TE 40 ms. An axial section was selected from the unenhanced images for dynamic MRI. A 0.1 mmol/kg bolus of Gd-DTPA was injected manually within 5 s, followed by a 20 ml saline flush. We used lipid suppression for subcutaneous fat, which can be superimposed on the brain because of large chemical-shift artefacts seen with GE EPI. All 17 patients were examined using multisection data acquisition, so as to cover the whole tumour. We acquired 5-section studies and 30 images of each section in 60 s periods. Each had section thickness of 5 mm, intersection gap 1 mm, 148×256 matrix, FOV 20×22 cm, TR 1.2, TE 46 ms. After data collection, the relative CBV maps were derived on a pixel-by-pixel basis from the dynamic image sets.

During the first pass of the bolus of contrast agent, T2* is reduced. The change in relaxation rate ($\Delta R2^*$) can be calculated from the signal intensity with the following equation: $\Delta R2^*(t) = \{-\ln[S(t)/S_0]\}/TE$, where S(t) is the signal intensity at time t, S_0 the preinjection signal intensity, and TE the echo time. $\Delta R2^*$ is proportional to the concentration of contrast medium in the tissue, and CBV to the area under the curve of $\Delta R2^*(t)$, provided there is no recirculation or leakage of contrast medium [20]. This function approximates the curve that would have been obtained without recirculation from the area under the curve rather than from the original data.

To avoid the risk of calculating the relative CBV from normal vessels, we initially investigated the serial $\Delta R2^*$ maps from arterial to venous phases as well as conventional MRI and then located the ROI within tumours. For calculation of the maximum relative CBV ratios of tumour, ROI consisting of more than 20 pixels were carefully chosen by a neuroradiologist, such that they did not include apparently cystic or necrotic areas, at contralateral white matter and over five regions of higher relative CBV. Then the maximum relative CBV ratios were calculated.

For multivoxel 2D CSI proton MRS, the volume of interest (VOI) chosen was confirmed by taking half-Fourier acquisition single-shot turbo-spin-echo (HASTE) images (TR 11.9, TE 95, TI 500 ms, one excitation). We obtained 19 5-mm sections with 38 s acquisition time in the axial, coronal and sagittal planes for all patients. We utilised an automated multivoxel 2D CSI sequence (TR 1500, TE 135 ms, PRESS double-spin echo) for MRS. This involved preselection of a volume within the brain, to prevent the strong interference from subcutaneous fat, which smaller than the phase-encode FOV, and must be large enough to prevent wrap-around artefacts. The CSI sequence produced a 16×16 transversely oriented matrix defined by phase encoding with FOV 16×16 cm. The plane was positioned to include the abnormality within the VOI resulting in maps of 8×8 spectra (VOI 8×8×1.5 cm^3). The field homogeneity achieved in automated nonlocalised multiple-angle projection (MAP) shimming resulted in water peak line-widths in the VOI typically <8 Hz. We collected spectral maps were collected with 2.56 ms sinc-hanning-shaped RF pulses for chemical shift selective excitation (CHESS) and subsequent spoiling of the resultant water signal. The second echo was collected by using 1024 data points and a spectral width of 500 Hz. All multivoxel PRESS 2D CSI measurements were one acquisition per phase-encode step with four prescans, TR 1500, TE 135 ms, acquisition time 12 min 55 s. After retrospective positioning of the VOI on the tumour, time domain data were multiplied with a Gaussian function (centre 0 ms, half-width 256 ms).

We estimated the areas of selected metabolite peaks such as choline-containing compounds (Cho), total creatine (Cr), N-acetylaspartate (NAA), the lactate doublet (Lac) and mobile lipids (Lip). Resonances were assigned as follows (ppm): Cho 3.21; Cr 3.04; NAA ; Lac 1.3; Lip 0.5–1.5 ppm. Lac assignment was observing the characteristic doublet caused by the inversion of the peak due to the J modulation. The peak area ratios of maximum Cho/NAA, Cho/Cr and minimum NAA/Cr within solid tumour regions were calculated. Since the area under the Cr peak is relatively constant in normal brain, its mean value was used as an internal standard or reference peak to estimate changes in the other metabolites. Each patient served as his or her own control. The normal regions were selected from a contralateral area or an area adjacent to the tumour site. We used three to five spectra to derive the mean values for Cho and Cr within normal regions (Cho-n, Cr-n). Then we calculated normal peak area ratios (Cho-n/Cr-n) and tumour Cho to normal Cr peak area ratios (Cho/Cr-n). The presence of Lac and/or Lip peaks within tumours was also sought.

We looked at correlations between the maximum relative CBV, minimum ADC and metabolite ratios (maximum Cho/NAA, Cho/Cr and Cho/Cr-n). We also investigated whether increased Cho levels or Cho-related metabolite ratios coincided with increased regional CBV or decreased ADC in the same patient.

Statistical analysis was performed using Statview 4.02 in Macintosh. An independent variable *t* test was used to determine differences between high- and low-grade gliomas in maximum relative CBV, the minimum ADC and metabolite ratios (maximum Cho/NAA, Cho/Cr, Cho/Cr-n, minimum NAA/Cr and mean Cho-n/Cr-n). We assessed correlations between maximum relative CBV, minimum ADC and metabolite ratios by correlation analysis, taking a P value of <0.05 as significant.

Results

All patients tolerated the DWI, proton MRS and perfusion sequences without producing motion artefacts and none had any adverse reaction to the rapid bolus injection of contrast medium. Conventional MRI findings are shown in Table 1. Table 2 summarises the maximum relative CBV, minimum ADC and metabolite peak area ratios.

There were three high-grade gliomas which showed little or no contrast enhancement. Necrosis was identified visually six glioblastomas and two anaplastic gliomas. Distant tumour foci, defined as discrete enhancing areas remote from the main tumour, were present only in two cases of glioblastoma.

Minimum ADC in the 13 high-grade gliomas was 0.51–1.55 ($\times 10^{-3}$ mm^2/s), mean 0.92 ± 0.27 ($\times 10^{-3}$ mm^2/s), while in the low-grade gliomas it varied from 1.06 to 1.37 ($\times 10^{-3}$ mm^2/s), mean 1.28 ± 0.15 ($\times 10^{-3}$ mm^2/s); this difference was statistically significant ($P < 0.05$). The minimum ADC in the eight patients with a glioblastoma was 0.51–0.96 ($\times 10^{-3}$ mm^2/s), mean 0.80 ± 0.14 ($\times 10^{-3}$ mm^2/s), whereas in the five patients with anaplastic gliomas it ranged from 0.76 to 1.6 ($\times 10^{-3}$ mm^2/s), with a mean 1.1 ± 0.31 ($\times 10^{-3}$ mm^2/s). This difference was also statistically significant ($P < 0.05$).

Maximum relative CBV was 1.70–16.17, mean 6.10 ± 3.98, in the 13 high-grade and 1.17–2.45, mean 1.74 ± 0.57, in the four low-grade gliomas; the difference was statistically significant ($P < 0.05$). In the eight patients

Table 1. Conventional MRI

Case/Age (years)/sex	Histology	Site	Necrosis	Contrast enhancement	Distant tumour foci	Heterogeneity	Cyst(s)	Definition of margins
1/17/F	Glioblastoma	Temporal	No	Minimal	No	Yes	No	Poor
2/33/M	Glioblastoma	Frontal	Yes	Extensive	No	Yes	No	Good
3/44/M	Glioblastoma	Insular cortex, temporal	Yes	Extensive spots	Yes	Yes	No	Poor
4/45/M	Glioblastoma	Temporal	Yes	Extensive	No	Yes	No	Poor
5/45/M	Glioblastoma	Frontal	Yes	Moderate	No	Yes	No	Good
6/55/M	Glioblastoma	Frontal, temporal	Yes	Extensive	Yes	Yes	No	Poor
7/ 63/F	Glioblastoma	Thalamus, temporal	No	Extensive	No	No	No	Poor
8/ 65/F	Glioblastoma	Thalamus, temporal	Yes	Extensive	No	Yes	No	Poor
9/16/M	Anaplastic astrocytoma	Thalamus-basal ganglia	No	Extensive spot	No	No	No	Poor
10/55/M	Anaplastic oligodendroglioma	Bilateral frontal	No	Absent	No	Yes	No	Poor
1/ 56/F	Anaplastic astrocytoma	Parietal	No	Absent	No	No	No	Good
12/60/M	Anaplastic oligodendroglioma	Frontal	Yes	Extensive	No	Yes	Yes	Poor
13/65/F	Anaplastic oligodendroglioma	Frontal	Yes	Extensive	No	Yes	No	Good
14/45/M	Low-grade astrocytoma	Parietal	No	Absent	No	No	No	Poor
15/50/M	Low-grade astrocytoma	Fronto-temporal	No	Absent	No	Yes	No	Poor
16/67/F	Oligoastrocytoma	Temporal	No	Moderate	No	Yes	Yes	Good
17/14/M	Subependymal giant-cell astrocytoma	Foramen of Monro	No	Moderate	No	No	No	Good

with glioblastoma it varied from 3.04 to 16.17, mean 7.26 ± 4.28, whereas in the five with anaplastic gliomas it was 1.70–8.79, mean 4.23 ± 2.89. This difference was not statistically significant ($P = 0.19$, Student's t test).

The mean metabolite rations in the high- and low-grade gliomas are shown in Table 3. Cho/Cr-n and Cho-n/Cr-n ratios could not be obtained in case 10, because the tumour was too large, and an 8×8 cm VOI could not be placed in normal brain. Significant differences between the high- and low-grade gliomas were found in all ratios, except for Cho-n/Cr-n ($P = 0.92$). No significant difference was found between glioblastomas and anaplastic gliomas for any metabolite ratio (all $P > 0.58$). An inverse doublet Lac peak was found in the solid part of four glioblastomas and three anaplastic gliomas, but not in any low-grade glioma. Lip peaks were found in four glioblastomas and two anaplastic gliomas, but none of the low-grade gliomas (Table 2).

A statistically significant inverse correlation was observed between relative CBV and ADC ($P = 0.008$, $R^2 = 0.38$), and between ADC and Cho/Cr-n peak area ratios ($P = 0.035$, $R^2 = 0.241$) (Fig. 1). However, no significant correlation was found between relative CBV and any metabolite peak area ratio.

Most patients showed good agreement among CBV map, ADC map and metabolite images (Figs. 2, 3). High-grade gliomas tended to have higher regional CBV, higher Cho/NAA, Cho/Cr, Cho/Cr-n ratios and lower ADC. However, in cases 5, 10, 11 and 16 there was disagreement between the CBV maps, ADC maps and metabolite images. In patient 5, with a glioblastoma, the maximum regional CBV was in the outer part of the tumour, but the minimum ADC and the maximum Cho/Cr ratio were found in its inner part. Lower CBV and higher ADC were found patients 10 and 11, with anaplastic gliomas, but both had high Cho/NAA and Cho/Cr ratios (Fig. 4).

Discussion

One important characteristic of malignant gliomas is their ability to infiltrate brain parenchyma. Infiltration is usually along the vascular channels of the white-matter tracts and spreads across the commissural fibres. This pathway allows distant tumour spread without disruption of the blood-brain barrier and with relative preservation of the underlying cytoarchitecture. Since contrast enhancement in conventional MRI indicates disruption of the blood-brain barrier and not underlying regional vascularity, it cannot be used alone to predict histological grade [7]. In this study, three high-grade

Table 2. Perfusion, diffusion and spectroscopic imaging. *Cho* choline *Cr* creatine *NAA* N-acetylaspartate *-n* in normal brain

Case	Histology	Maximum relative cerebral blood volume	Maximum apparent diffusion coefficient ($\times 10^{-3}$ mm^2/s)	Maximum Cho/NAA	Maximum NAA/Cr	Minimum NAA/Cr	Maximum Cho/Cr-n	Mean Cho-n/Cr-n	Lactate	Lipid	Agreement[a]
1	Glioblastoma	5.21	0.790	7.1	10.75	0.38	3.18	0.98	+	+	+
2	Glioblastoma	16.17	0.956	5.06	2.69	0.30	2.26	0.97	+	+	+
3	Glioblastoma	5.31	0.784	5.04	3.15	0.43	2.29	0.96	+	+	+
4	Glioblastoma	4.98	0.906	5.64	5.61	0.44	2.81	0.89	–	–	+
5	Glioblastoma	11.10	0.514	4.93	2.71	0.35	2.55	1.04	–	–	–
6	Glioblastoma	6.33	0.874	9.06	4.65	0.40	2.45	0.99	–	–	+
7	Glioblastoma	6.20	0.713	5.71	5.15	0.34	3.13	0.90	–	+	+
8	Glioblastoma	3.04	0.825	4.39	3.07	0.48	2.44	0.92	+	–	+
9	Anaplastic astrocytoma	4.77	0.918	12.86	6.09	0.34	4.01	0.86	–	–	+
10	Anaplastic oligodendroglioma	1.70	1.250	5.11	4.26	0.35	/	/	+	–	–
11	Anaplastic astrocytoma	1.81	1.554	5.73	4.35	0.46	2.23	1.02	+	+	–
12	Anaplastic oligodendroglioma	4.10	1.156	2.97	2.76	0.49	1.89	1.06	–	–	+
13	Anaplastic oligodendroglioma	8.79	0.755	3.04	6.23	0.41	3.68	0.97	+	+	+
14	Low-grade astrocytoma	1.17	1.334	1.04	2.44	2.05	3.35	1.10	–	–	+
15	Low-grade astrocytoma	1.41	1.374	2.19	1.52	0.45	1.18	0.94	–	–	+
16	Oligoastrocytoma	2.45	1.343	0.10	0.32	3.75	0.27	0.95	–	–	–
17	Subependymal giant-cell astrocytoma	1.94	1.057	3.25	3.08	0.34	1.63	0.92	–	–	+

[a]between regional cerebral blood volume map, apparent diffusion coefficient map and metabolite imaging

Table 3. Tumour metabolites

Grade of glioma	Metabolite rations (mean ± SD)				
	Maximum Cho/NAA	Maximum Cho/Cr	Maximum Cho/Cr-n	Minimum NAA/Cr	Cho-n/Cr-n
High	5.90 ± 2.62	4.73 ± 2.22	2.66 ± 0.68	0.40 ± 0.06	0.96 ± 0.06
Low	1.65 ± 1.37	1.84 ± 1.20	1.61 ± 1.29	1.65 ± 1.61	0.98 ± 0.08
P	0.0077	0.0266	0.0445	0.0083	0.7177

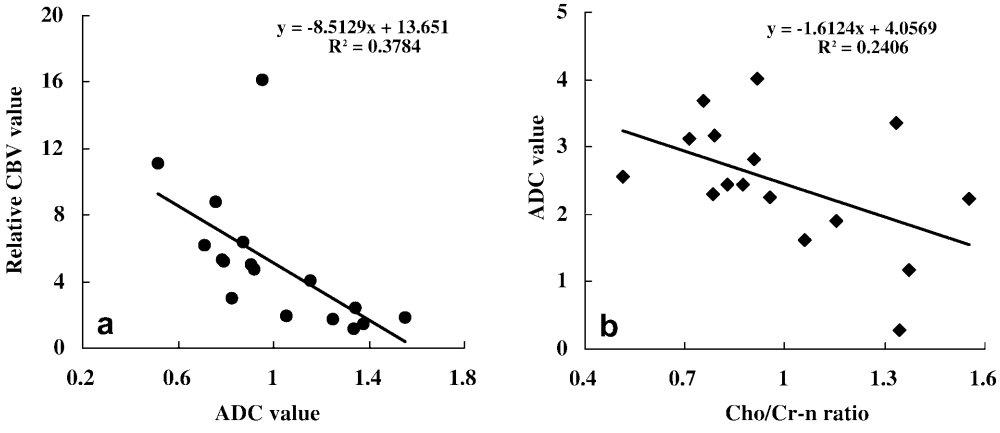

Fig. 1a, b. Correlation plots. **a** Maximum relative cerebral blood volume (CBV) versus minimum apparent diffusion coefficient (ADC). **b** Minimum ADC versus tumour choline peak (Cho)/normal brain creatine (Cr-n) ratio

gliomas showed little or no enhancement. Previous reports have documented that tumour grade is not always related to oedema, heterogeneity, necrosis, cyst formation, definition of borders, haemorrhage or mass effect [6, 7]. In this study, necrosis, heterogeneity and definition of the margins of the tumour could not be used to differentiate high- and low-grade gliomas. Conventional MRI was thus unreliable.

Histologically, gliomas demonstrate considerable heterogeneity, with focal areas of more malignant features dispersed over regions with a less aggressive appearance. These histologically unrepresentative regions are observed to a very variable extent in different patients, particularly in high-grade gliomas. Ideally, gliomas should be graded using specimens from their most malignant portion.

Dynamic susceptibility-contrast MRI has been developed to obtain images of regional CBV. Perfusion methods have been used to create regional CBV maps in normal brain and in tumours [6, 9, 16, 20, 21]. Aronen et al. [6] demonstrated that high-grade gliomas often contain areas of increased and decreased blood volume, while low-grade gliomas are typically more homogeneous, with decreased blood volume. High regional CBV is more likely in high-grade tumours [7, 22]. The relative CBV, although not an absolute measure of regional blood volume, can reflect tumour vascularity and may be a better indicator of histological grade. Most of our high-grade gliomas showed higher maximum relative CBV than the low-grade tumours, with a significant difference between the high- and low-grade groups.

The magnitude and direction of diffusion of tissue water depend on the permeability and spacing of diffusion barriers, the viscosity of the suspending medium, and the duration of observation [23]. Quantitative information on restriction of movement of water molecules can be obtained by calculating the ADC. Published data on intracranial tumours indicate that high ADC were attributable to low cellularity, necrosis or cysts, and lower values to dense, highly cellular tumour [24, 25]. The ADC was $< 1.5\times10^{-3}$ mm^2/s in a patient with a cerebral astrocytoma [26] and $< 2.0\times10^{-3}$ mm^2/s in another with an oligodendroglioma [27]. Brunberg et al.[18], using a motion-insensitive spin-echo sequence in three orthogonal directions, reported a mean ADC of 1.38×10^{-3} mm^2/s in cerebral oedema, 1.31×10^{-3} mm^2/s in solid, enhancing central tumour and at the tumour margin, and 2.35×10^{-3} mm^2/s in cyst or necrosis. We found the minimum ADC to be lower in the high-grade gliomas than in low-grade tumours, a result similar to those of previous reports.

Most previous studies used one diffusion gradient direction (z-axis) when calculating the ADC. However, normal white matter has been reported to consistently show diffusion anisotropy; water is relatively unrestricted along the white-matter tracts but more restricted orthogonal to them [28]. For this reason, the white matter orientated in the direction of the diffusion gradient has a higher ADC, whereas the white matter orthogonal to it has a markedly lower ADC. Theoretically, invariant anisotropy indices can be calculated from the six estimated diffusion tensor elements [29]. However,

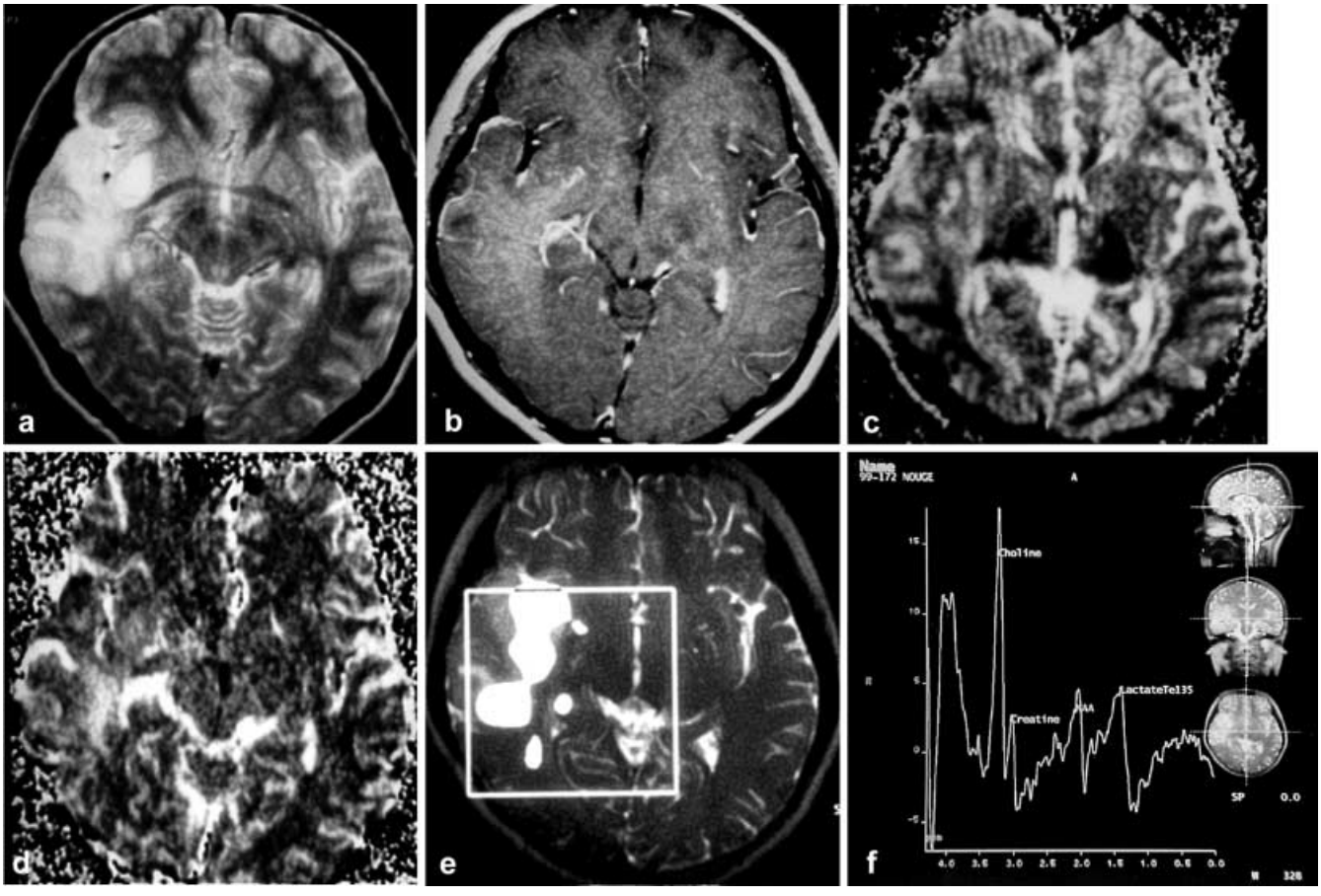

Fig. 2a–f. Case 1: a 17-year-old girl with a glioblastoma multiforme. **a** Axial T2-weighted MRI shows an ill-defined high-signal mass in the right temporal lobe. **b** A contrast-enhanced image with minimal enhancement. **c, d** The mass shows low ADC and high relative CBV value in the ADC and relative CBV maps. **e** The Cho/Cr ratio distribution map shows a high ratio (*bright*) in the region of the mass. **f** Proton MR spectrum from the posterior part of the mass shows increased Cho, decreased N-acetylaspartate (NAA) and Cr peaks. An inverse doublet lactate peak at 1.3 ppm and increased lipid peak at 1.5 ppm are clearly seen

the mean minimum ADC used in this study is proportional and used to eliminate the affect of anisotropy of brain white matter by the derivation of diffusion coefficients from the x, y, and z axes of the imager in present clinical applications [18, 19].

Recent years have seen increased emphasis on studying the metabolic activity of brain lesions for diagnostic purposes and for monitoring treatment. Several studies have shown that common features of many rapidly growing tumours are an increased Cho/Cr ratio, a decreased NAA/Cr ratio and an increased Lac level [12, 30, 31]. Studies using proton MRS indicate a similar correlation between metabolic features in vivo and the histological grade of gliomas [32, 33, 34, 35], and indicated that lactate is more likely to be present in high-grade tumours [31, 32, 35]. Lipids were recognised in vivo in 23% of the spectra from 48 gliomas and it was suggested that they are more frequent in higher-grade tumours [35]. This would agree with the finding that intact surgical specimens of higher-grade gliomas contain mobile lipids, the amounts of which correlate with the extent of cell necrosis on microscopy [36].

In all published studies, metabolic signal intensities showed large variations and overlaps between histological grades. Moreover, trends in metabolic changes in different grades were inconsistent. Some reports indicate that the Cho/Cr ratio does not increase progressively with higher grades [32, 37, 38]; the level of NAA did not decrease progressively with increasing grade, but was higher in high-grade than in intermediate grade gliomas, and higher in the latter than in low-grade tumours [31, 35, 38, 39]. Factors which may contribute to variations in results from different studies include: nonuniformity of techniques used to localise the proton spectra to the region of interest; variable attempts to avoid contamination of spectra by metabolites from oedematous brain and obviously nonviable parts of tumours; and different acquisition parameters, in particular, echo and repetition times.

Multivoxel methods can be useful for obtaining a metabolic map of a large lesion or brain region. With

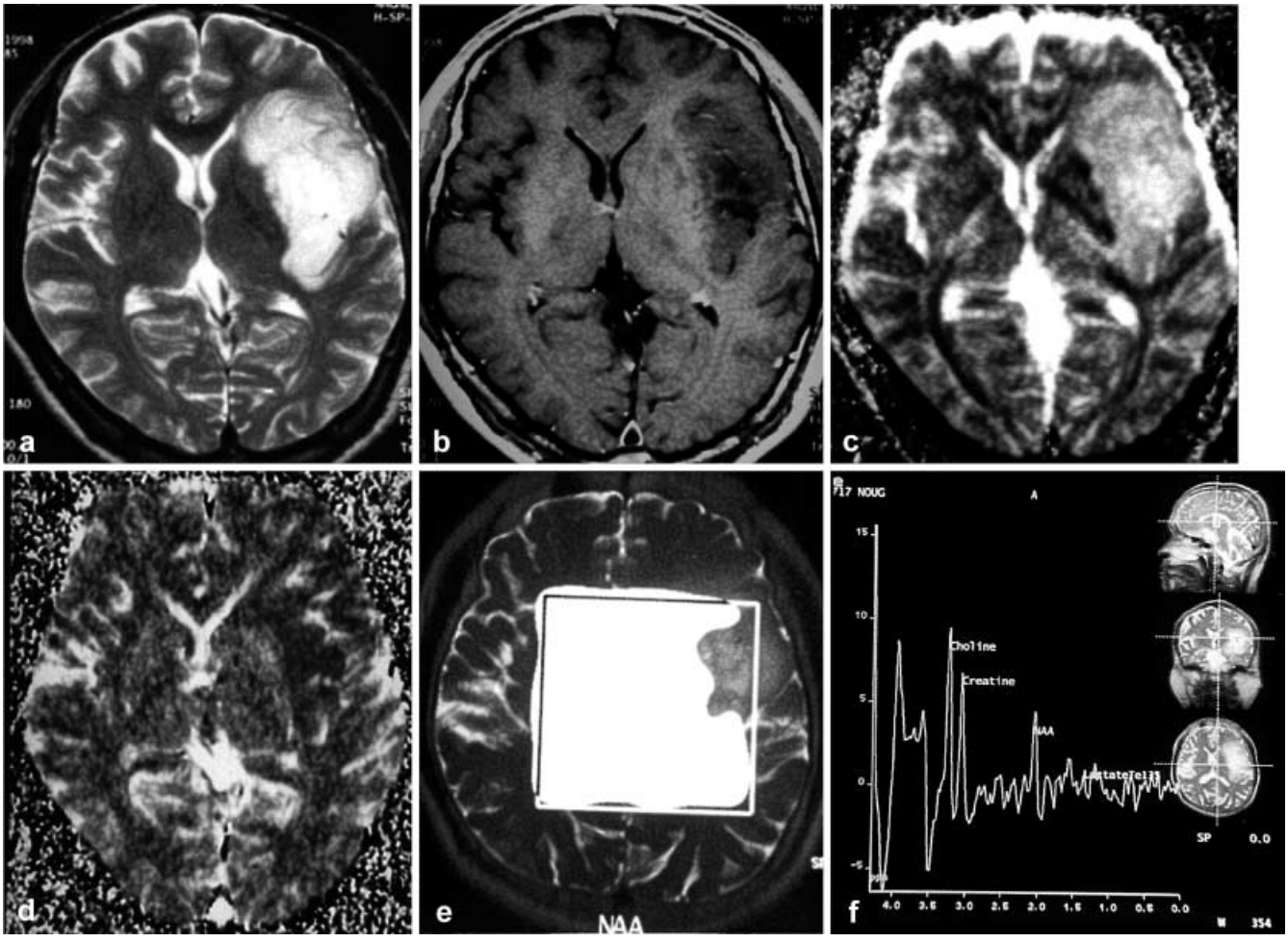

Fig. 3a–f. Case 15: a 50-year-old man with a low-grade astrocytoma. **a** Axial T2-weighted MRI shows a high-signal mass in the left frontotemporal region. **b** A contrast-enhanced image demonstrates no enhancement. **, c, d** The ADC and relative CBV maps show high and low values, respectively. **e** An NAA distribution map shows decreased levels. **f** Proton MRS from the posterior part of the mass shows increased Cho and decreased NAA peaks. No lactate (1.3 ppm) or lipid (1.0–1.5 ppm) peaks are present

these techniques, voxels containing viable tumour can be identified a priori. Our data show that tumour grades can be differentiated with a high degree of precision using the multivoxel CSI technique. The ratios of maximum Cho/NAA, Cho/Cr, Cho/Cr-n and minimum NAA/Cr are highly correlated with tumour grade, but no significant difference was found between glioblastomas and anaplastic gliomas. No Lac or Lip peak was detected in the solid part of low-grade tumours, and the latter was found only in high-grade gliomas. This suggests that Lip and Lac peaks may have discriminatory power. Large amounts of lipids appear to be specific for anaplastic gliomas or glioblastomas, but their absence does not exclude either. Because the presence of mobile lipids in high-grade astrocytomas correlates with cell necrosis [40] and the latter with prognosis [4], it is possible that mobile lipids in anaplastic gliomas will be a marker for tumours likely to exhibit more aggressive behaviour.

From a biological perspective, tumour cellularity and vascularity may be related. We used both DWI and perfusion MRI to look at cerebral gliomas study, and found a statistically significant inverse correlation between maximum relative CBV and minimum ADC. However, in case 5 we saw a different pattern, in which the maximum regional CBV was at the margin of the lesion and the minimum ADC in its inner part. It could, therefore, be argued that the tissue with a high cellularity (lower ADC) may have limited blood supply.

Only one previous study [17] has used diffusion MRI and proton MRS together to investigate human intracranial gliomas. A statistically significant inverse correlation between the Cho signal intensities and the ADC was found in radiologically defined tumour-containing regions. This inverse correlation suggests that tumour-cell density plays a major role in defining the level of Cho signal on MRS. Gupta et al. [17] also suggested that even the more cellular portions of intracranial gliomas

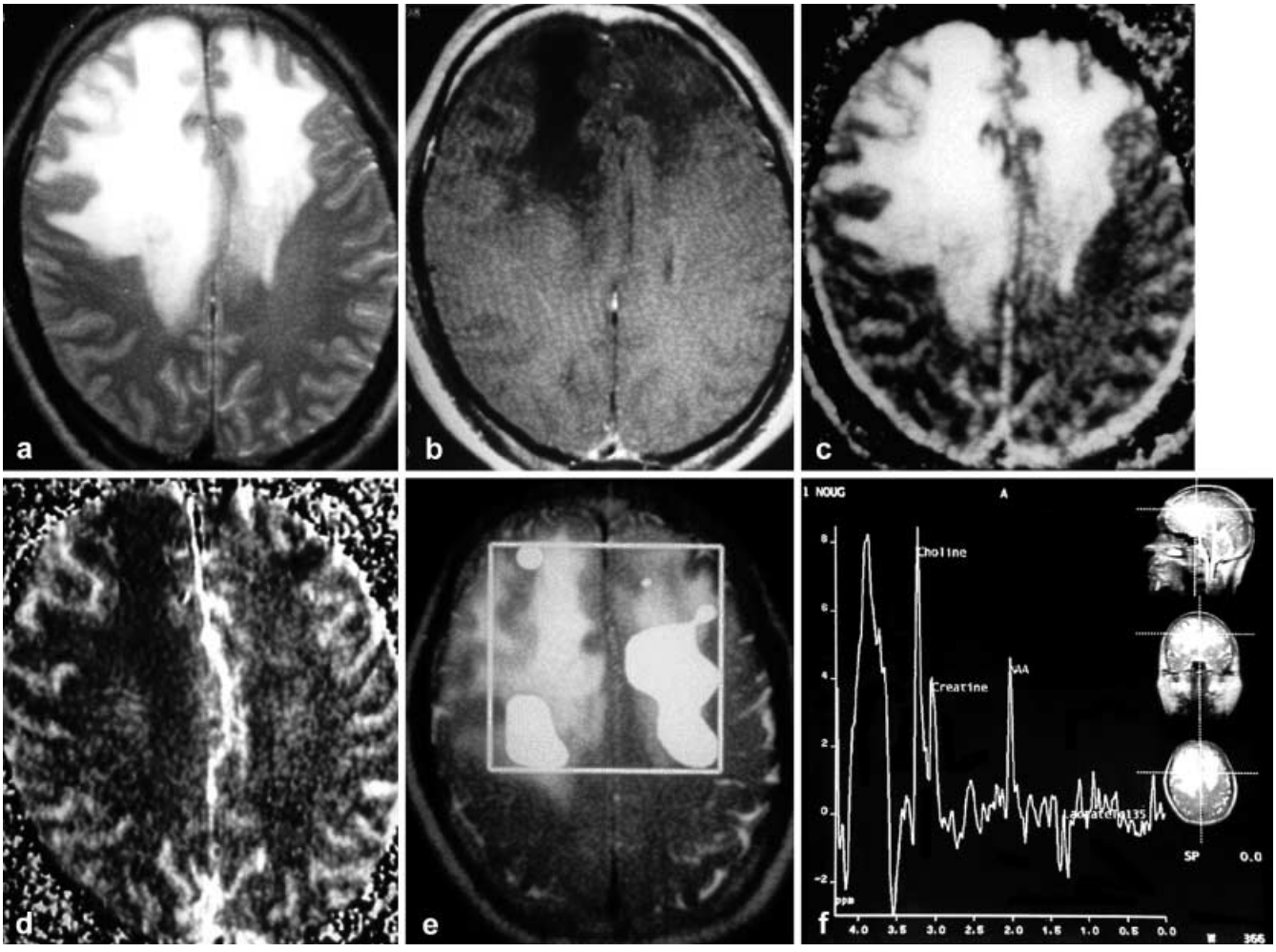

Fig. 4a–f. Case 10: a 55-year-old man with an anaplastic oligoastrocytoma. **a** Axial T2-weighted MRI demonstrates a diffuse high-signal mass in both frontal lobes. **b** There is no contrast enhancement. **c, d** ADC and relative CBV maps show high ADC and slightly increased relative CBV. **e** The Cho/Cr ratio distribution map shows a high ratio (*bright*) in the posterior part of the mass. **f** Proton MRS from the posterior part of the mass shows increased Cho, and decreased NAA and Cr peaks. An inverse doublet lactate peak at 1.3 ppm is clearly seen

tend to have somewhat higher ADC than normal tissue. This would be consistent with a relatively large extracellular volume associated with micronecrosis and interstitial oedema, even in the more cellular tumour components. However, radiation-induced cell membrane damage may change the levels of membrane phosphocholine [41], and more than half the patients in the earlier study had undergone radiotherapy.

We saw an inverse correlation between Cho/Cr-n and the ADC. Although Cho/Cr-n is not the absolute value of choline, we believe it can reflect its metabolism, since the area under the Cr peak is relatively constant in normal brain. We therefore consider that our data indicate a statistically significant inverse correlation between ADC and increased levels of choline. The association between phosphocholine increase and cell proliferation is often attributed to acceleration of membrane and phospholipid metabolism. Many studies have demonstrated that phosphocholine levels are elevated in actively proliferating cells and that this can be measured noninvasively with ^{31}P- or ^{1}H-MRS [42, 43, 44]. However, the inverse correlation is imperfect: some tumour voxels which appeared to have a relatively higher cellularity as indicated by their ADC also showed higher Cho/Cr-n ratios. The two anaplastic gliomas, in which MRS was more useful than DWI, had high ADC and high Cho/Cr-n ratios. However, we may postulate that the very aggressive tumour voxels have both high cellularity and high proliferative potential, although it may be questioned whether spectroscopically measured total Cho levels in glioma should on the proliferative potential. We believe that DWI and MRS may indeed complement each other in assessment of cerebral gliomas.

We have shown good correlations between maximum relative CBV and minimum ADC, and between

minimum ADC and metabolic ratios in the histological grading of gliomas. Direct comparison of each image obtained by perfusion imaging, DWI and MRS offered more detailed information on the complicated intra- and peritumoral architecture that reflect tumour vascularity, cellularity and metabolic information on cellularity and proliferation, respectively. EPI perfusion MRI, DWI and multivoxel 2D CSI proton MRS can offer useful diagnostic information, not available from conventional MRI alone, in preoperative assessment of glioma grades. The DWI, perfusion MRI and proton MRS do indeed complement each other.

References

1. Kaba SE, Kyritsis AP (1997) Recognition and management of gliomas. Drugs 53: 235–244
2. Rees JH, Smirniotopoulos JG, Jones RV, et al (1996) Glioblastoma multiforme: radiologic-pathologic correlation. Radiographics 16: 1413–1438
3. Daumas-Duport C, Scheithauer B, O'Fallon J, Kelly P (1988) Grading of astrocytomas: a simple and reproducible method. Cancer 62: 2152–2165
4. Burger PC, Vogel FS, Green SB, Staike TA (1985) Glioblastoma multiforme and anaplastic astrocytoma: pathologic criteria and prognostic implications. Cancer 56: 1106–1111
5. Felix R, Schorner W, Laniado M, Niendorf HP, et al (1985) Brain tumors: MR imaging with gadolinium-DTPA. Radiology 156: 681–688
6. Aronen HJ, Gazit IE, Louis DV, et al (1994) Cerebral blood volume maps of gliomas: comparison with tumor grade and histologic findings. Radiology 191: 41–51
7. Knopp EA, Cha S, Johnson G, et al (1999) Glial neoplasms: dynamic contrast-enhanced T2*-weighted MR imaging. Radiology 211: 791–798
8. Belliveau JW, Rosen BR, Kantor HL, et al (1990) Functional cerebral imaging by susceptibility-contrast NMR. Magn Reson Med 14,538–546
9. Edelman RR, Mattle HP, Atkinson DJ, et al (1990) Cerebral blood flow: assessment with dynamic contrast-enhanced T2*-weighted MR imaging at 1.5 T. Radiology 176: 211–220
10. Pierpaoli C, Jezzard P, Basser P, et al (1996) Diffusion tensor MR imaging of the human brain. Radiology 201: 637–648
11. Cousins JP (1995) Clinical MR spectroscopy: fundamentals, current applications, and future potential. Am J Roentgenol 164: 1337–1347
12. Poptani H, Gupta RK, Roy R, et al (1995) Characterization of intracranial mass lesions with in vivo proton MR spectroscopy. AJNR 16: 1593–1603
13. Vigneron DB, Nelson SJ, Murphy-Boesch J, et al (1990) Chemical shift imaging of human brain: axial, sagittal, and coronal P-31 metabolite images. Radiology 177: 643–649
14. Wald L, Moyher S, Day M, Nelson S, Vigneron D (1995) Proton spectroscopic imaging of the human brain using brain phased array detectors. Magn Reson Med 34: 440–445
15. Prost R, Haughton V, Li SJ (1997) Brain tumors: localized H-1 MR spectroscopy at 0.5 T. Radiology 204: 235–238
16. Tzika AA, Vajapeyam S, Barnes PD (1997) Multivoxel proton MR spectroscopy and hemodynamic MR imaging of childhood brain tumors: preliminary observations. AJNR 18: 203–218
17. Gupta RK, Sinha U, Cloughesy TF, Alger JR (1999) Inverse correlation between choline magnetic resonance spectroscopy signal intensity and the apparent diffusion coefficient in human glioma. Magn Reson Med 41: 2–7
18. Brunberg JA, Chenevert TL, McKeever PE, et al (1995) In vivo MR determination of water diffusion coefficients and diffusion anisotropy: correlation with structural alteration in gliomas of the cerebral hemispheres. AJNR 16: 361–371
19. Bammer R, Stollberger R, Augustin M, et al (1999) Diffusion-weighted imaging with navigated interleaved echo-planar imaging and a conventional gradient system. Radiology 211: 799–806
20. Rosen BR, Belliveau JW, Vevea JW, et al (1990) Perfusion imaging with NMR contrast agents. Magn Reson Med 14: 249–265
21. Maeda M, Itoh S, Kimura H, et al (1993) Tumor vascularity in the brain: evaluation with dynamic susceptibility-contrast MR imaging. Radiology 189: 233–238
22. Sugahara T, Korogi Y, Kochi M, et al (1998) Correlation of MR imaging-determined cerebral blood volume maps with histologic and angiographic determination of vascularity of gliomas. Am J Roentgenol 171: 1479–1486
23. Tanner JE (1983) Intracellular diffusion of water. Arch Biochem Biophys 224: 416–428
24. Tien R, Felsberg GJ, Friedman H, et al (1994) MR imaging of high-grade cerebral gliomas: value of diffusion-weighted echoplanar pulse sequences. Am J Roentgenol 162: 671–677
25. Sugahara T, Korogi Y, Kochi M, et al (1999) Usefulness of diffusion-weighted MRI with echo-planar technique in the evaluation of cellularity in gliomas. J Magn Reson 9: 53–60
26. Le Bihan D, Breton E, Lallemand D, et al (1986) MR imaging of intravoxel incoherent motions: application to diffusion and perfusion in neurologic disorders. Radiology 161: 401–407
27. Hajnal JV, Doran M, Hall AS, et al (1991) MR imaging of anisotropically restricted diffusion of water in the nervous system: technical, anatomic, and pathologic considerations. J Comput Assist Tomogr 15: 1–18
28. Chenevert TL, Brunberg JA, Pipe JG (1990) Anisotropic diffusion in human white matter: demonstration with MR techniques in vivo. Radiology 177: 401–405
29. Pierpaoli C, Basser PJ (1996) Toward a quantitative assessment of diffusion anisotropy. Magn Reson Med 36: 893–906
30. Tedeschi G, Lundbom N, Raman R, et al (1997) Increased choline signal coinciding with malignant degeneration of cerebral gliomas: a serial proton magnetic resonance spectroscopy imaging study. J Neurosurg 87: 516–524
31. Usenius JP, Kauppinen RA, Vainio PA, et al (1994) Quantitative metabolite patterns of human brain tumors: detection by ^{1}H NMR spectroscopy in vivo and in vitro. J Comput Assist Tomogr 18: 705–713
32. Fulham MJ, Bizzi A, Dietz MJ, et al (1992) Mapping of brain tumor metabolites with proton MR spectroscopic imaging: clinical relevance. Radiology 185: 675–686

33. Shimizu H, Kumabe T, Tominaga T, et al (1996) Noninvasive evaluation of malignancy of brain tumors with proton MR spectroscopy. AJNR 17: 737–747
34. Meyerand ME, Pipas M, Mamourian A, et al (1999) Classification of biopsy-confirmed brain tumors using single-voxel MR spectroscopy. AJNR 20: 117–123
35. Ott D, Hennig J, Ernst T (1993) Human brain tumors: assessment with in vivo proton MR spectroscopy. Radiology 186: 745–752
36. Kuesel AC, Sutherland GR, Halliday W, Smith IC (1994) 1H MRS of high grade astrocytomas: mobile lipid accumulation in necrotic tissue. NMR Biomed 7: 149–155
37. Demaerel P, Johannik K, van Hecke P, et al (1991) Localized ^{1}H NMR spectroscopy in fifty cases of newly diagnosed intracranial tumors. J Comput Assist Tomogr 15: 67–76
38. Kugel H, Heindel W, Ernestus RI, et al (1992) Human brain tumors: spectral patterns detected with localized H-1 MR spectroscopy. Radiology 183: 701–709
39. Arnold DL, Shoubridge EA, Villemure JG, et al (1990) Proton and phosphorus magnetic resonance spectroscopy of human astrocytomas in vivo. Preliminary observations on tumor grading. NMR Biomed 3: 184–189
40. Kuesel AC, Donnelly SM, Halliday W, et al (1994) Mobile lipids and metabolic heterogeneity of brain tumors as detectable by ex vivo ^{1}H NMR spectroscopy. NMR Biomed 7: 172–180
41. Gillies RJ, Barry JA, Ross BD (1994) In vitro and in vivo 13C and 31P NMR analyses of phosphocholine metabolism in rat glioma cells. Magn Reson Med 32: 310–318
42. Aiken NR, Szwergold ES, Kappler F, et al (1996) Metabolism of phosphonium choline by rat-2 fibroblasts: effects of mitogenic stimulation studied using ^{31}P NMR spectroscopy. Anticancer Res 16: 1357–1363
43. Mahmood U, Alfieri AA, Thaler H, et al (1994) Radiation dose-dependent changes in tumor metabolism measured by 31P nuclear magnetic resonance spectroscopy. Cancer Res 54: 4885–4891
44. Aiken NR, Gillies RJ (1996) Phosphomonoester metabolism as a function of cell proliferative status and exogenous precursors. Anticancer Res 16: 1393–1397